FUDMA Journal of Engineering and Technology
ISSN: 3092-9385
https://fjet.fudutsinma.edu.ng/index.php/fjet/
Volume 2, Issue 1, 2026, 784-794

# Design and Simulation of a Synchronous Reference Frame-Based Active Power filter for Harmonic Mitigation

Olusegun A. AFOLABI[1*], Olanrewaju A. OLANITE[2], Nsikan L. AKPAN[3]

[1*,3]Department of Electrical/Electronic Engineering Technology, Federal Polytechnic Mubi, Adamawa State, Nigeria
[2]Department of Electrical/Electronic Engineering, Niger State Polytechnic, Zungeru, Niger State, Nigeria

[1*]afolabiolusegunabioye@gmail.com, [2]olaniteolanrewaju@gmail.com, [3]chynsikan@gmail.com

***Abstract***

*The daily increase in the application of power electronics in modern devices is of serious concern. Power electronic or non-linear load devices such as battery charging systems, draw non-sinusoidal currents which tend to have a detrimental impact on the power quality of distribution systems. The use of these devices badly distorts the current waveforms in the system's supply. In order to reduce harmonic distortion in a three-phase distribution system delivering nonlinear loads, this study examines the design and performance of a shunt Active Power Filter (APF). Power quality and system efficiency are negatively impacted by the substantial current harmonics introduced by the growing prevalence of power electronic devices. To address this issue, an APF based on synchronous reference frame (SRF) control is developed and implemented in a 3-phase, 11 kV/400 V, 500 kVA system. By using hysteresis current control and Synchronous Reference Frame (dq0) transformation, the suggested control approach allows for precise harmonic component extraction and correction.MATLAB/Simulink is used to assess the system performance, and the Fast Fourier Transform (FFT) is used for harmonic analysis. Total Demand Distortion (TDD) and individual harmonic limitations are used to evaluate compliance with IEEE 519 standards. According to simulation results, TDD significantly decreased from 24.76% to 0.73%, much below the recommended 8% limit. The results verify that the suggested APF arrangement is successful in delivering high-quality power under nonlinear loading circumstances.*

***Keywords:*** *Active Power Filter, Harmonic Mitigation, IEEE519 Standard, Nonlinear load, Total Harmonic Distortion (THD).*

## 1.0 Introduction

The world's electrical energy consumption has recently surged due to population growth, the electrification of industrial operations like automobiles, and the behaviour of new consumers toward the advancement of technology[1]. As a result, high-power quality indices and responsible energy use are receiving more attention. Avoiding and reducing various AC issues, such as frequency fluctuation and Total Harmonic Distortion THD, is advantageous for power networks. However, with growing nonlinear loads, AC distributed power networks have encountered numerous difficulties in ensuring and enhancing the necessary level of power quality indices [2]. Enhancing the effectiveness of power filters for better device and network performance has garnered more attention in recent years.

Current and voltage harmonic sources are the two primary forms of harmonic distortions that generally result in a nonlinear load [3]. Furthermore, non-linear loads increase total harmonic distortions (THDs), power transmission-line losses, and power factors. Reducing the THD is a crucial and primary duty in power systems to enhance the electrical system's power quality. Power filters have been researched and applied in recent years to reduce the power grid's THD. Power filters can be broadly classified into three categories: hybrid active power filter (HAPF), active power filter (APF), and passive power filter (PPF) [4]. Nevertheless, the limited capacity to track the dynamic behaviour of nonlinear loads is a drawback of employing PPFs in the power network. APF uses voltage source inverters, which are more efficient, less expensive, and smaller than current source inverters, in addition to three-phase pulse width modulation (PWM) to address this issue[5].

This study attempts to develop and simulate an Active Power Filter (APF) with an optimal control topology that can respond to the system harmonics and reduce them to the smallest fractions of the set standard in order to meet the IEEE519 standard limits for current harmonics.

## 2.0 Materials and Methods

This study models a highly inductive load as a harmonic source that is fed from a 3-Ø, 11 kV/400 V, 50 Hz supply. A synchronous reference frame (SRF) theory is essentially used in the modelling of the APF[6]. For a more straightforward explanation, this theory converts the three-phase stationary frame to a two-phase rotational frame. The load's harmonic content is taken from the analysis, reversed, and then reinjected into the system for nullification of the same magnitude. The IEEE Std 519 Harmonic Limits for current harmonics, which are

Received: 22/04/2026; Revised: 13/05/2026; Accepted: 15/05/2026; Published: 23/05/2026

displayed in Table 1, were used as a reference line to assess the filter's performance on the system harmonics. MATLAB/Simulink was used to simulate and execute the filter design. The Simulink software's Fast Fourier Transform (FFT) signal processing toolbox was used to analyse the system's harmonic distortions.

Table 1: IEEE Std 519 Harmonic Limits

| **Current Distortion Limits in IEEE STD 519 for system Rated 120 V through 69 kV** | | | | | | |
|---|---|---|---|---|---|---|
| **Maximum Harmonic current distortion in Percent of $I_L$** | | | | | | |
| **Individual Harmonic order (Odd Harmonics)** | | | | | | |
| SCR ($I_{SC}/I_{L)}$ | 3≤h<11 | 11≤h<17 | 17≤h<23 | 23≤h<35 | 35≤h<50 | TDD |
| <20 | 4.0 | 2.00 | 1.50 | 0.60 | 0.3 | 5.0 |
| 20<50 | 7.0 | 3.50 | 2.50 | 1.00 | 0.5 | 8.0 |
| 50< 100 | 10.0 | 4.50 | 4.00 | 1.50 | 0.7 | 12.0 |
| 100< 1000 | 12.0 | 5.50 | 5.00 | 2.00 | 1.0 | 15.0 |
| >1000 | 15.0 | 7.00 | 6.00 | 2.50 | 1.4 | 20.0 |

Individual harmonics are prioritised over total harmonic distortion (THD) in the IEEE519 standard. Determining the load current's short circuit ratio (SCR) at the point of common coupling (PCC) is thus the first method in this standard[7].

SCR is calculated as shown in Equation (1).

$$SCR = \frac{I_{SC}}{I_L} \quad (1)$$

where $I_L$, the maximum load current = 26.53A, and Isc is the maximum short circuit current at PCC = 650.1A.

Typically, the utility provides Isc. It is ascertained in this study by taking a direct measurement of the current under no-load conditions as shown in Equation (2).

∴ 650.1/26.53 = 24.5 is the SCR. (2)

According to Table 1, this ratio suggests that the load current should meet each SCR's specific harmonic requirement within the range of 20 to 50. To examine the harmonic state at the moment, the present harmonic spectrum, which is displayed in Table 3, is obtained by FFT analysis.

### 2.1 The APF Design for Harmonic Elimination

A three-phase, three-wire shunt active power filter (APF) that injects a three-phase filter current into the power system at the point of common coupling is schematically depicted in Figure 1.

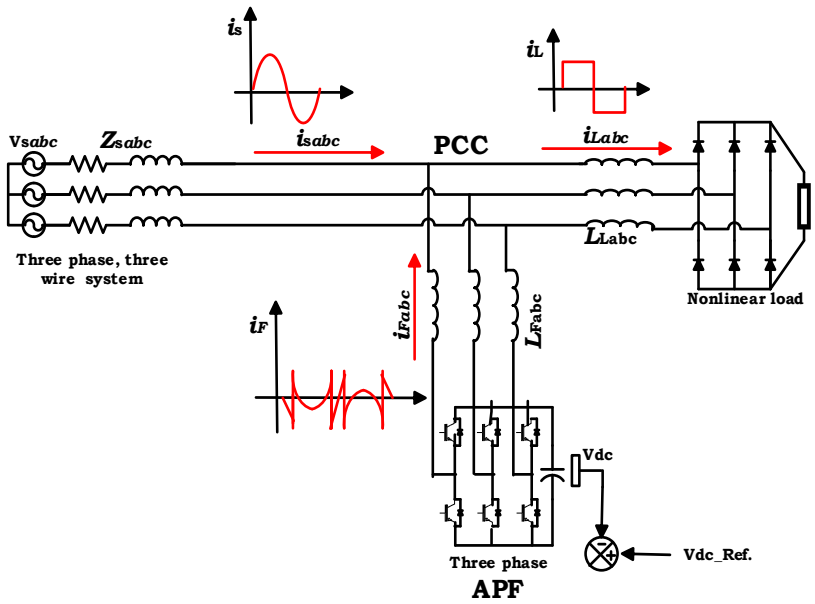


Figure 1: Shunt active power filter schematic diagram

Three primary tasks are involved in harmonic elimination using this filter: i*abc, reference current generation, hysteresis control approach for tracking reference currents, and optimal regulation of the DC-link voltage of the filter voltage source converter (VSC).

### 2.2 Generating Reference Current Using Synchronous Reference Frame (dq0) Theory

The following steps effectively estimate the three-phase reference currents:

• Conversions of the three-phase load currents (iLabc) and source voltages (VSabc). This is accomplished by applying the synchronous reference frame theory, which is essentially the conversion of three-phase system values to two reference frames by Clark and Park. Using a low-pass filter (LPF), harmonic components are extracted.

• To get identical three-phase reference currents, take the inverse of the transformed iLabc. Figure 2 shows the control algorithm and operation of SAPF that illustrated this procedure as well as the remaining filter control steps.

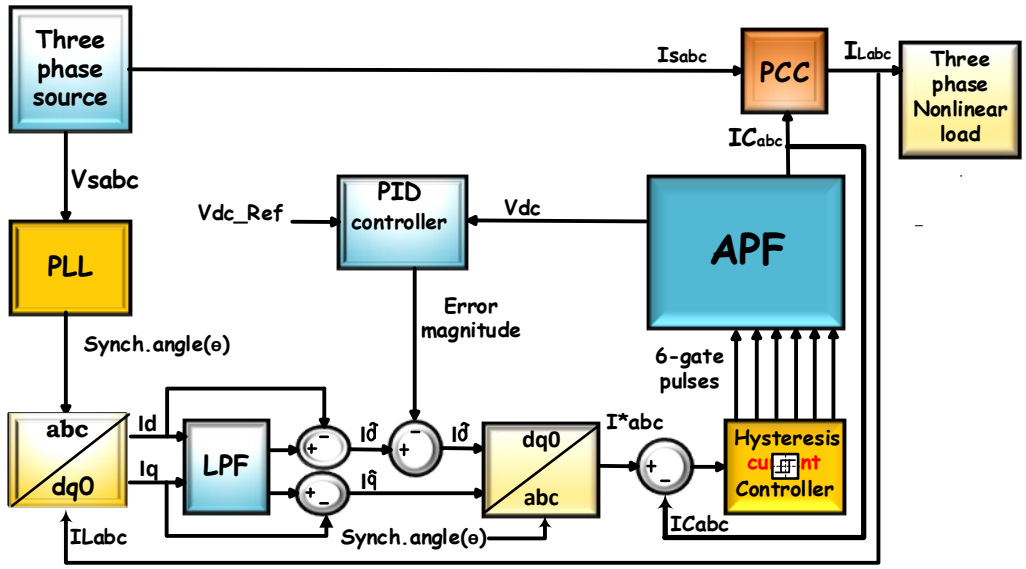


Figure 2: Control algorithmand operation of SAPF

### 3.0 Blocks of Transformation

The oscillating components of the currents are necessary to offset the harmonic contents in the load currents iLabc. Consequently, a precise and simple mathematical model is required. Even though it can be difficult to mathematically model a dynamic electrical system with time-varying voltages and currents, such a complicated system can be readily made simpler with a few basic mathematical adjustments[8]. Every one of the time-dependent variables is made simpler in relation to a single reference variable. Park's and Clark's transformation approaches are used in this context. The geometric representation in Figure 3 (a) illustrates how the three-phase ABC quantities are decoupled into a two-phase orthogonal system in a stationary reference frame known as the αβ frame in Clark's transformation. The orthogonal stationary reference frame αβ is further converted into a rotating reference frame called dq using Park's transformation, as shown in Figure. 3 (b).

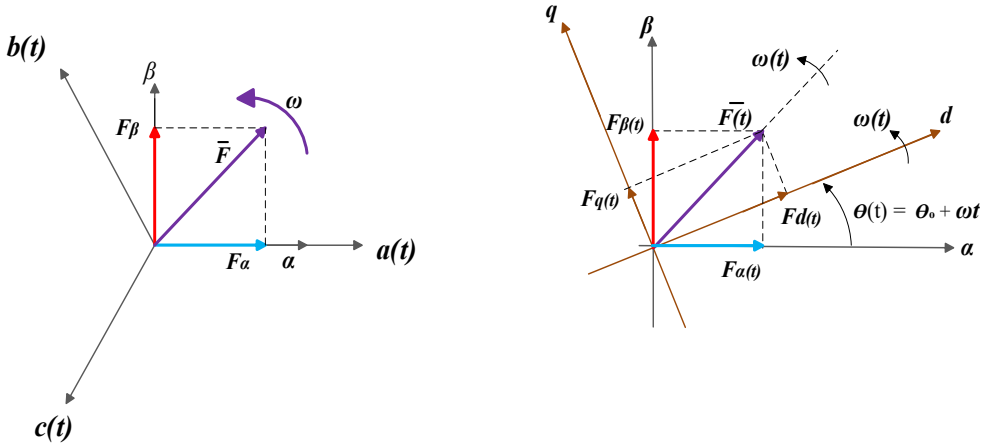


(a) αβ0 reference frame (b) dq0 reference frame

Figure 3: Clark's and Park's transformation geometric representation

Received: 22/04/2026; Revised: 13/05/2026; Accepted: 15/05/2026; Published: 23/05/2026

$$\begin{bmatrix} F_0 \\ F_\alpha \\ F_\beta \end{bmatrix} = \sqrt{\frac{2}{3}} \begin{bmatrix} \frac{1}{\sqrt{2}} & \frac{1}{\sqrt{2}} & \frac{1}{\sqrt{2}} \\ 1 & -\frac{1}{\sqrt{2}} & -\frac{1}{\sqrt{2}} \\ 0 & \frac{\sqrt{3}}{2} & \frac{\sqrt{3}}{2} \end{bmatrix} \begin{bmatrix} F_a \\ F_b \\ F_c \end{bmatrix} \quad (3)$$

The three-phase stationary vectors Fa, Fb, and Fc in the ABC frame are converted into the two-phase, αβ orthogonal reference frame's Fα and Fβ stationary vectors in Fig. 2.3(a). For a balanced three-phase system, the third component, F0, is a zero-sequence component vector that equals zero. Similarly, the projections in Figure 3(b) resolve the transformation of the αβ frame to a spinning dq frame. The projection of q is along the q-axis and perpendicular to that of d, as this figure illustrates. The direct component is denoted by "d," and the quadrature component by "q." The unit vector Fd(t) is moved from the α-axis at ωt at an angle θ. Equation 3 displays the transformation matrix that is derived from this data.

$$\begin{bmatrix} F_d \\ F_q \\ F_0 \end{bmatrix} = \begin{bmatrix} \cos(\omega t) & \sin(\omega t) & 0 \\ -\sin(\omega t) 1 & \cos(\omega t) & 0 \\ 0 & 0 & 1 \end{bmatrix} \begin{bmatrix} F_\alpha \\ F_\beta \\ F_0 \end{bmatrix} \quad (4)$$

The dynamic frequency in radians is denoted by ω. This unit vector is considered synchronised with the rotating dq coordinate system if it rotates at a system frequency of 50 Hz. With regard to this dq system, this rotational vector—which may be either voltage or current—will be fixed and constant (DC).
To keep things simple, equation 4 is a different way to represent Park's transformation, which is created straight from the ABC frame (i.e., by combining equations 2 and 3).

$$F_{dq0} = \frac{2}{3} \begin{bmatrix} \cos\theta & \cos(\theta - \frac{2\pi}{3}) & \cos(\theta + \frac{2\pi}{3}) \\ \sin\theta & \sin(\theta - \frac{2\pi}{3}) & \sin(\theta + \frac{2\pi}{3}) \\ \frac{1}{2} & \frac{1}{2} & \frac{1}{2} \end{bmatrix} F_{abc} \quad (5)$$

These analyses produce dq quantities, Id and Iq rotating at ω(t), from the three-phase load currents iLabc as displayed in the block diagram of Figure 2. These currents are basically DC for a balanced three-phase linear load, with a synchronisation angle that is tracked by the phase lock loop (PLL) and no ripples. However, as Figures 4 (a) and (b) demonstrate, oscillatory components are imposed on the net current vectors due to the presence of harmonics.

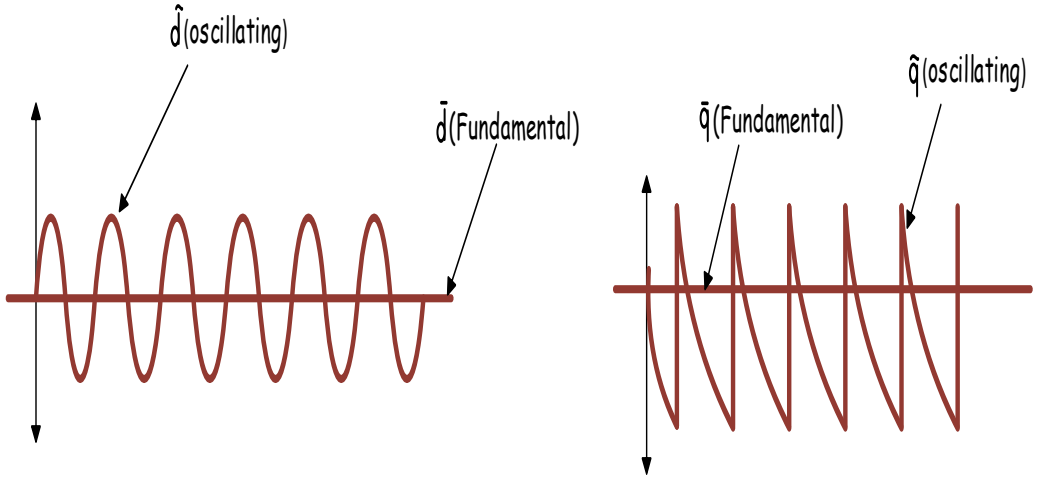


(a) Active Current Signal (b) Reactive Current Signal
Figure 4: Fundamental and oscillating components of load currents in a dq-frame

The active (d-axis) component of load current referenced to one of the phases is shown in Figure 4(a). A DC or fundamental () and an oscillating or harmonic content () make up this current vector. Similarly, as illustrated in Figure 4 (b), the reactive (q-axis) component of the load consists of both fundamental () and harmonic (). The reference currents generated by these harmonic components are then monitored for the APF converter gate firing signal.

Received: 22/04/2026; Revised: 13/05/2026; Accepted: 15/05/2026; Published: 23/05/2026 

### 3.1 Inverse Clark Transformation Block

This block determines the corresponding three-phase reference currents, i*abc. This is done by taking the reciprocal of the dq components of the oscillating current. Equations (6) below are essentially the inverse of Clark's transformation as shown in Equation (5).

$$\begin{aligned} i_a^* &= i_{\mathrm{d}}\, sin\theta + i_{\mathrm{q}}\, cos\theta \\ i_b^* &= i_{\mathrm{d}}\, sin\left(\theta - \frac{2\pi}{3}\right) + i_{\mathrm{q}}\, cos\left(\theta - \frac{2\pi}{3}\right) \\ i_c^* &= i_{\mathrm{d}}\, sin\left(\theta - \frac{2\pi}{3}\right) + i_{\mathrm{q}}\, cos\left(\theta + \frac{2\pi}{3}\right) \end{aligned} \qquad (6)$$

### 4.0 DC bus Voltage Tracking using PID controller

The DC bus voltage needs to be maintained at a specific level in order to provide an appropriate harmonic compensation current. On the other hand, the voltage source inverter injects filter current (IFabc) into the system when the Active Power Filter (APF) is operating by converting AC to DC at a very high switching frequency. Power is lost as a result of the inverter's alternating switching. Additionally, power loss is also caused by the interface reactor. Therefore, to guarantee that power is maintained across the switches, the DC link voltage is placed. However, because this DC bus voltage is derived from a capacitor, it can collapse after a few seconds.

A proportional integral differential controller (PID) is used in a control algorithm to maintain a constant DC voltage. By maintaining the Vdc as close to the reference Vdc as feasible, this controller guarantees that the Vdc error is zero. The constants Kp and KI have values of 0.5 and 50, respectively, based on the PID controller's tuned response.

When the voltage dips owing to internal power losses, the inverter turns a portion of the source currents into DC to charge the capacitor back to its reference value. The active part of the Sinusoidal current is the primary cause of the coupling reactance losses and internal switching losses in the VSI; this is the cumulative steady state error that the PID controller discovers. The total reference current is calculated by adding this mean error to the oscillating component of Id. These reference currents are the ones that must be managed to produce driving signals for the inverter switches' gates. The inverse of Clark's transformation is represented by the three-phase reference currents, i*abc.

### 5.0 Reference Currents Tracking Using Hysteresis Control Technique

The following stage involves creating firing signals for the APF inverter using the reference currents that have been established. This indicates that the reference currents will be followed by the inverter when it is run. This is accomplished by comparing the reference current i*abc with the actual inverter current iCabc to produce switching. The resulting 3-phase error signals are then regulated within a bandwidth or region defined by this error signal.

By doing this, the ripple contents will be contained to a small range. This is crucial, particularly for applications requiring high dynamic performance like motor drives. The literature has a variety of inverter current control methods, including hysteresis current control and triangular carrier current control. The hysteresis current control strategy[9] is employed in this study because of its straightforward design and effective operation. By restricting the ripple contents within a hysteresis region, this method adjusts the inverter to ensure the average variation of the current is nearly sinusoidal. A πrad sinusoidal reference current (phase a) and a boundary are depicted next to the reference current in the diagram of figure 5.

Received: 22/04/2026; Revised: 13/05/2026; Accepted: 15/05/2026; Published: 23/05/2026 

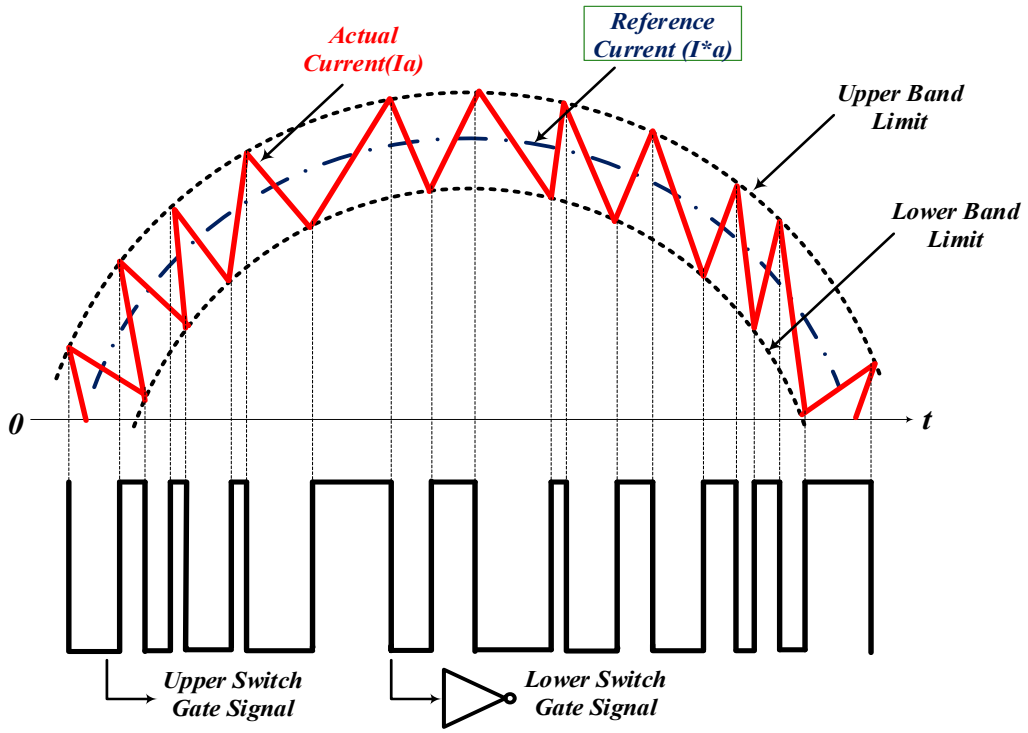


Figure 5: Hysteresis current control technique

A half-cycle sinusoidal signal and its matching pulse-width-modulated signal are depicted in the diagram. The hysteresis band described in the paragraph that follows shows that the upper and lower switches are turned on and off in a complementary manner. For example, the top switch turns OFF and the lower switch turns ON if the actual current (ia) reaches the upper band; otherwise, the upper switch turns OFF and the lower switch turns ON. To put it another way, the inverter's top switch shuts off and its lower switch turns on alternately if ia < i*a. The bandwidth is adjusted to avoid being too narrow or too wide. Fast and fine tracking can be achieved with a smaller width, but the switching frequency will increase. Conversely, poor tracking results from a broad bandwidth, but switching losses are reduced due to the decreased switching frequency. The bandwidth used in this study is chosen between -0.01 and 0.001. The hit-and-trial approach for the closest sinusoidal resolution is used to get the bandwidth.

## 6.0 Design simulation using MATLAB/Simulink Software

MATLAB/Simulink software is used to verify the filter's harmonic mitigation performance based on the design parameters and mathematical theories outlined in Table 2. Figure 6 displays the filter's MATLAB/Simulink model. Four main subsystems make up the model: (1) the supply system, the load system, the mitigation device, and its control system. PCC is used to define a location where the harmonic limits are to be applied. In other words, it's a bus that provides access to the system for the compensating currents.

Table 2: Simulation design parameters

| **Parameters** | **Description** |
|---|---|
| Load | DC, RL Load |
| Inverter Rating | 40kVA (Max) |
| Inverter DC bus voltage | 653V |
| Inverter DC bus capacitor | 6000μF |
| Supply | 3-Ø, 11kV/400V, 500kVA transformer, 50Hz, impedance 1Ω,1mH |
| Coupling inductor | 1.2mH |

Received: 22/04/2026; Revised: 13/05/2026; Accepted: 15/05/2026; Published: 23/05/2026 

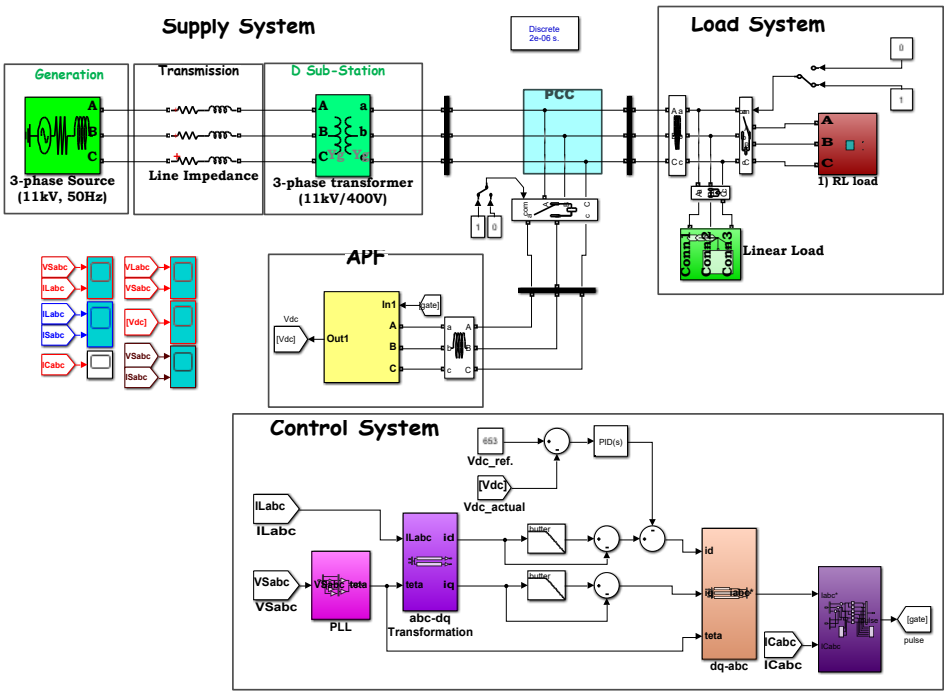


Figure 6: MATLAB simulation model for the AFP

## 7.0 Results and Discussion

Discussion of results with the illustrations of the simulation as presented in Figure 6 using the simulation parameters of Table 2 is presented in this section.

### 7.1 Results

#### 7.1.1 APF Control System Signals Waveform

The signal waveforms of the APF during different phases of its control system are displayed in Figure 7 (a) through (f). Park's transition of the load current from a three-phase, ABC stationary frame to a two-phase, dq0 rotational frame is depicted in Figure 7. (a) and (b). Since there is currently only a linear load connected, the currents in (a) appear to be DC. However, because a nonlinear load has been added to the system, there are some ripples in the currents in (b).

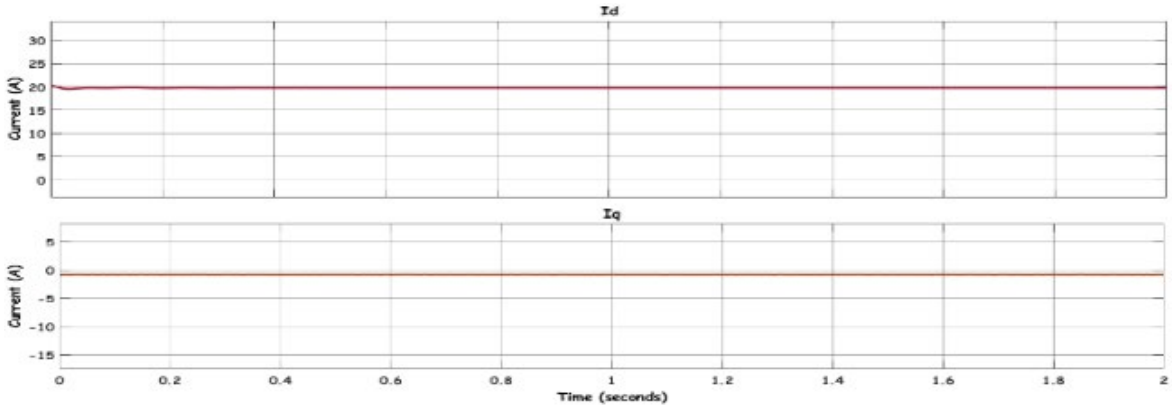


Figure 7 (a): Load current component in a qd-frame for the case of a linear load

Received: 22/04/2026; Revised: 13/05/2026; Accepted: 15/05/2026; Published: 23/05/2026 

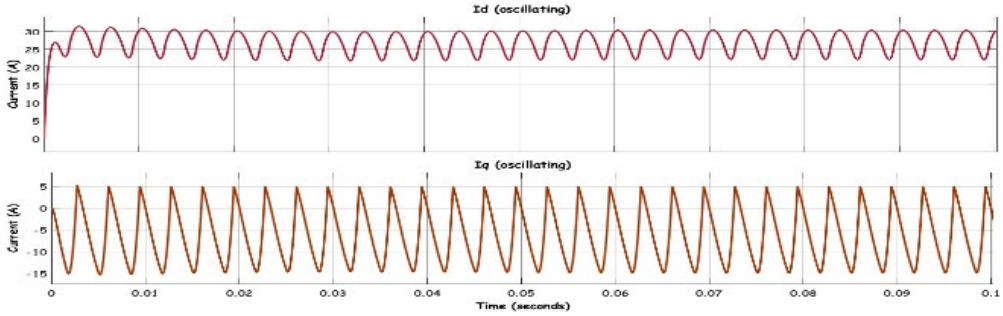


Figure 7 (b): Load current component in a qd-frame for the case of a nonlinear load.

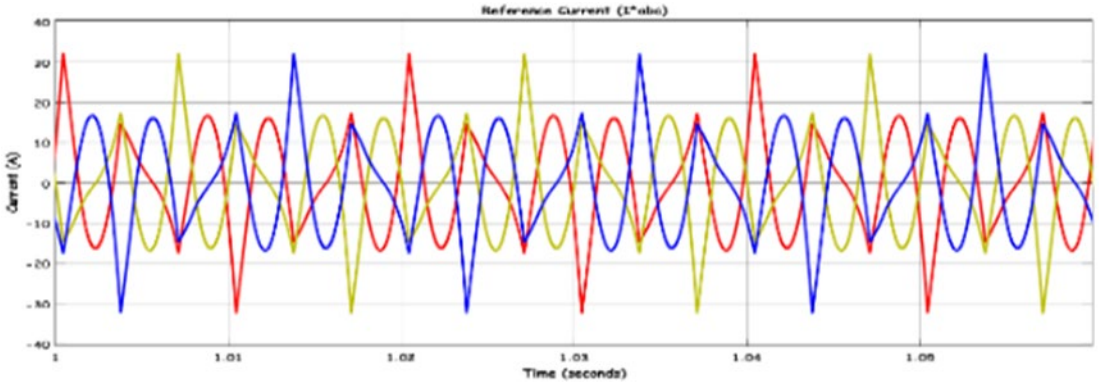


Figure 7 (c):Reference currents, I*abc

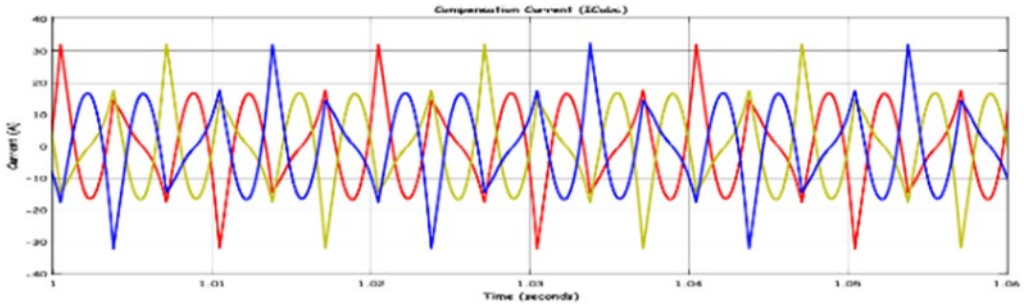


Figure 7 (d):APF compensation currents

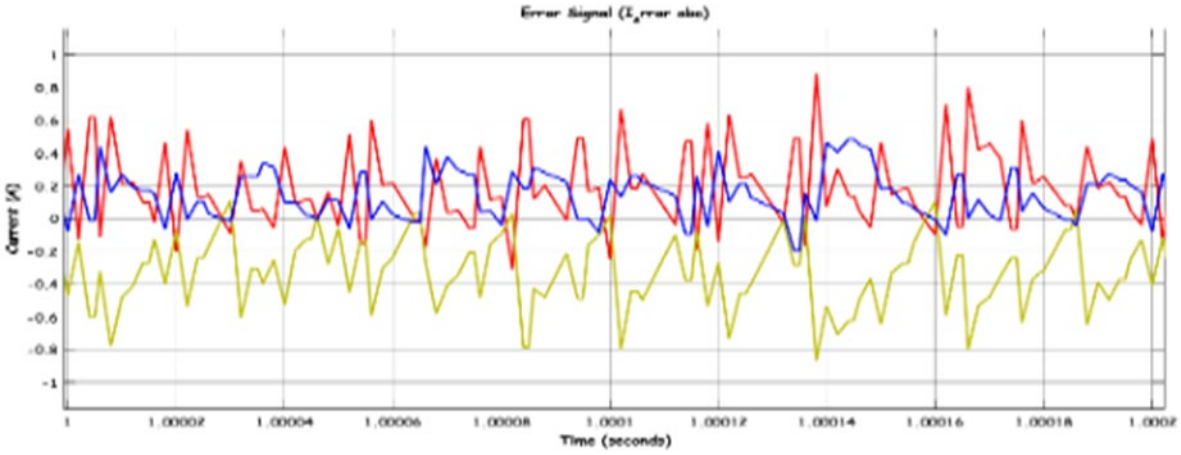


Figure 7 (e):Error signal waveforms

Received: 22/04/2026; Revised: 13/05/2026; Accepted: 15/05/2026; Published: 23/05/2026 

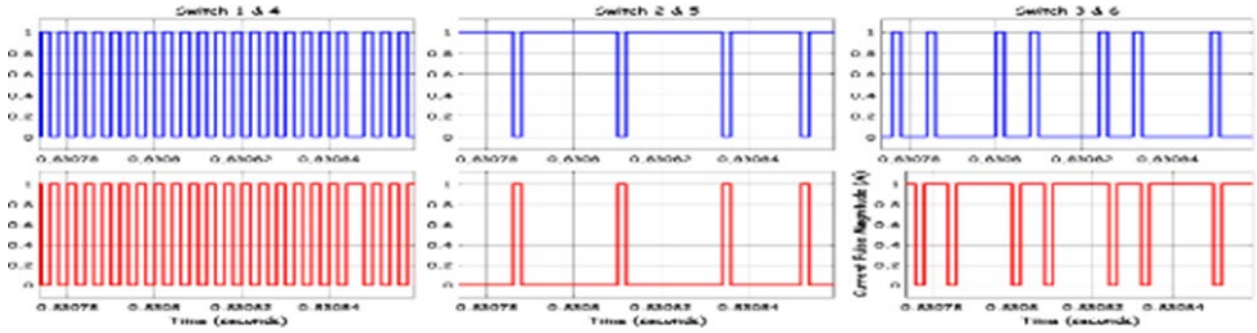


Figure 7 (f):Six-pulse PMW modulated APF

### 7.1.2 The load signals and FFT analysis before and after Mitigation

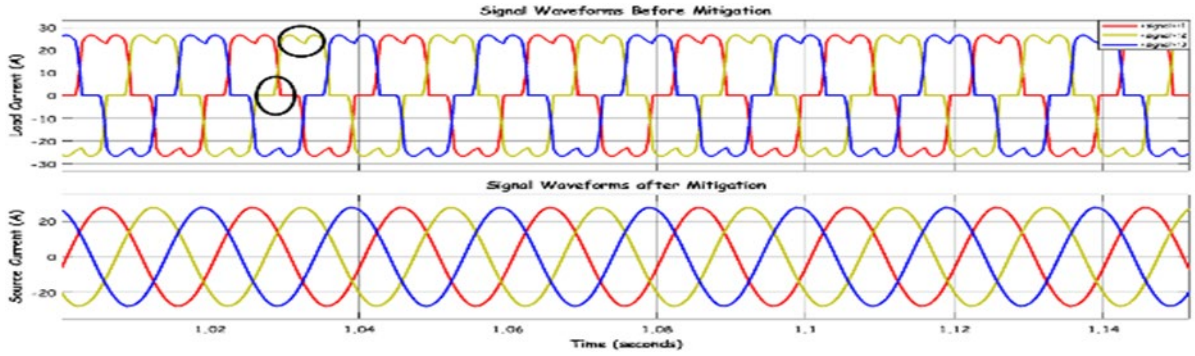


Figure 8 (a): Current output waveforms before and after mitigation

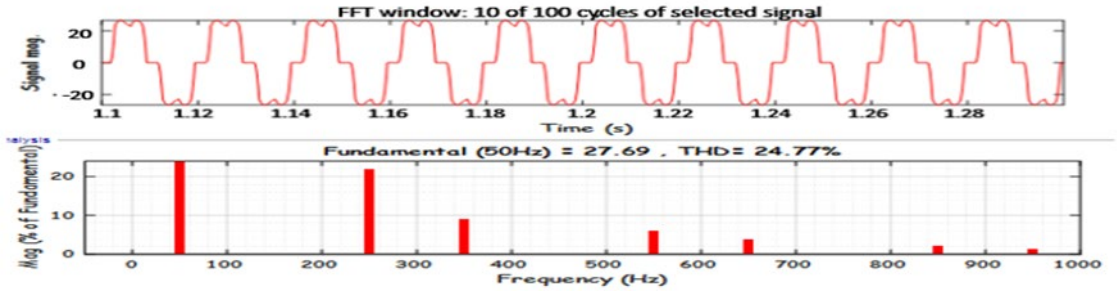


Figure 8 (b):FFT analysis before mitigation

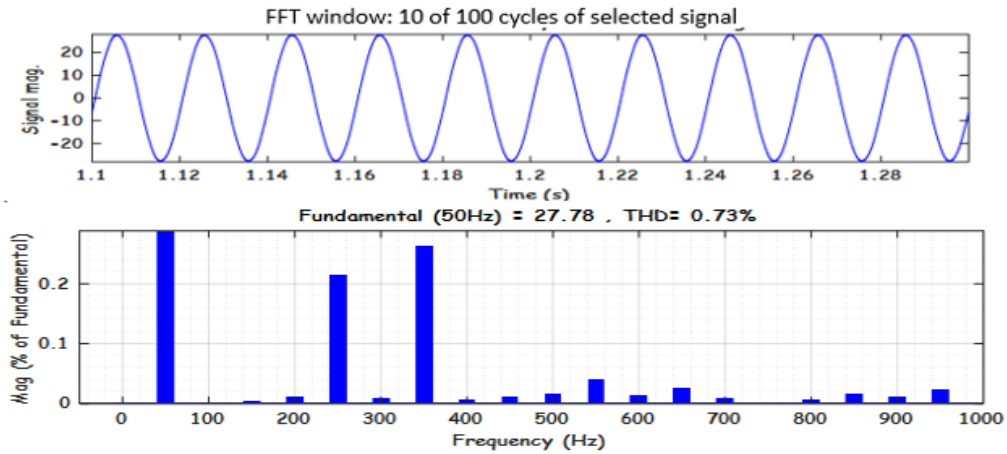


Figure 8 (c):FFT analysis after mitigation

Received: 22/04/2026; Revised: 13/05/2026; Accepted: 15/05/2026; Published: 23/05/2026 

**7.1.3 Simulink FFT analysis of the load Harmonic Distortion (%)**

Table 3 shows the percentage distortion for each odd harmonic from 7th to 19th as derived from the Fast Fourier Transform (FFT) analysis of Figure 8.

Table 3: Harmonic Condition of the system before and after incorporating APF

| **Harmonic Distortion (%)** | | | |
|---|---|---|---|
| **TDD & Harmonic order** | *Before Mitigation* | *After Mitigation* | *IEEE519 Standard (%) For SCR* **20<50** |
| TDD | 24.760 * | 0.730 √ | 8.00 |
| $h_5$ | 21.750 * | 0.221 √ | 7.00 |
| $h_7$ | 8.953 * | 0.276 √ | 7.00 |
| $h_{11}$ | 6.064 * | 0.041 √ | 3.50 |
| $h_{13}$ | 3.677 * | 0.044 √ | 3.50 |
| $h_{17}$ | 2.104√ | 0.023√√ | 2.50 |
| $h_{19}$ | 1.477√ | 0.029√√ | 2.50 |

## 8.0 Analysis

The system load state before and after incorporating the Filter is displayed in Table 3. The system harmonic load situation before filtering is shown in column two, while the matching IEEE519 standard limitations are shown in column four. As seen in column four, it is evident that the TDD and the individual harmonics from the fifth, seventh, eleventh, and thirteenth harmonics have been suppressed to the lowest fractions. Because they all occur in the zero sequence, which is absent from a three-phase, three-wire system, the odd harmonics in multiples of three do not exist for this load state. Following the connection of APF, which results in a significant suppression of certain frequencies, column three displays the % harmonic distortion results.

Although the 17th and 19th harmonics were already below their limits, the filter's connection resulted in a noticeable improvement. Passive filters can also produce similar results, albeit they are limited to certain harmonic frequencies that are practically unnecessary in a system with fluctuating loads. However, this technology has successfully mitigated all the higher-order harmonics in the system.

## 9.0 Conclusion

The development and the investigation of the impact of APF on system harmonic mitigation have been successfully completed in accordance with the study's objective. Therefore, all of the desired harmonic frequencies have been effectively removed. As a result, the system's current harmonics remain much below the IEEE 519 standard limits.

Voltage imbalance can also distort the supply system by causing a negative sequence component in the source voltage. Therefore, it is advised that a sensing circuit be included in future research to guarantee the fundamental voltage's positive sequence.

This study contributes to the existing body of knowledge in the following ways:

1. It offers a thorough implementation of a synchronous reference frame-based APF designed for a medium-voltage distribution system (11 kV/400 V), which is less commonly covered in previous research.
2. It demonstrate a significant reduction in Total Demand Distortion (TDD) from 24.76% to 0.73%, well below IEEE 519 limitations, demonstrating high-efficiency harmonic mitigation under realistic nonlinear load situations.
3. It combines hysteresis current control with SRF-based harmonic extraction, offering a straightforward control architecture with robust dynamic performance.
4. It offers a comprehensive MATLAB/Simulink simulation framework that can be used as a reproducible reference for future studies and real-world applications.

## References

[1] C. Albea, A. Sferlazza, F. Gomez-Estern, and F. Gordillo, "Hybrid Modelling and Control of a Class of Power Converters with Triangular-Carrier PWM Inputs," *IEEE Access*, vol. 9, pp. 151607–151620, 2021, doi: 10.1109/ACCESS.2021.3126433.

[2] M. L. Duc, L. Hlavaty, P. Bilik, and R. Martinek, "Harmonic Mitigation Using Meta-Heuristic Optimization for Shunt Adaptive Power Filters: A Review," *Energies*, vol. 16, no. 10, pp. 1–55, 2023, doi: 10.3390/en16103998.

[3] A. A. El-Ela, S. M. Allam, A. A. Mubarak, and R. A. El-Sehiemy, "Harmonic Mitigation by Optimal Allocation of Tuned Passive Filter in Distribution System," *Energy Power Eng.*, vol. 14, no. 07, pp. 291–312, 2022, doi: 10.4236/epe.2022.147016.

Received: 22/04/2026; Revised: 13/05/2026; Accepted: 15/05/2026; Published: 23/05/2026 

[4] K. Srilakshmi *et al.*, "Optimal design of solar/wind/battery and EV fed UPQC for power quality and power flow management using enhanced most valuable player algorithm," *Front. Energy Res.*, vol. 11, no. January, 2023, doi: 10.3389/fenrg.2023.1342085.

[5] F. Alasali, K. Nusair, H. Foudeh, W. Holderbaum, A. Vinayagam, and A. Aziz, "Modern Optimal Controllers for Hybrid Active Power Filter to Minimize Harmonic Distortion," *Electron.*, vol. 11, no. 9, 2022, doi: 10.3390/electronics11091453.

[6] H. Y. and M. R. R. Ali Dastfan, "Optimum Design of Passive Harmonic Filter by Using Game Theory Concepts," *Intell. Syst. Electr. Eng. J.*, vol. 4, no. 4, 2022.

[7] A. Cervone, M. Slunjski, E. Levi, and G. Brando, "Optimal Third-Harmonic Current Injection for Asymmetrical Multiphase Permanent Magnet Synchronous Machines," *IEEE Trans. Ind. Electron.*, vol. 68, no. 4, pp. 2772–2783, 2021, doi: 10.1109/TIE.2020.2982099.

[8] S. Agrawal, D. K. Palwalia, and M. Kumar, "Performance Analysis of ANN Based three-phase four-wire Shunt Active Power Filter for Harmonic Mitigation under Distorted Supply Voltage Conditions," *IETE J. Res.*, vol. 68, no. 1, pp. 566–574, 2022, doi: 10.1080/03772063.2019.1617198.

[9] M. Bajaj, N. K. Sharma, M. Pushkarna, H. Malik, M. A. Alotaibi, and A. Almutairi, "Optimal Design of Passive Power Filter Using Multi-Objective Pareto-Based Firefly Algorithm and Analysis under Background and Load-Side's Nonlinearity," *IEEE Access*, vol. 9, pp. 22724–22744, 2021, doi: 10.1109/ACCESS.2021.3055774.

Received: 22/04/2026; Revised: 13/05/2026; Accepted: 15/05/2026; Published: 23/05/2026 